

Studies on Accuracy of Numerical Simulations of Emission from Rough Ocean-Like Surfaces

Lin Zhou, *Student Member, IEEE*, Leung Tsang, *Fellow, IEEE*, Vikram Jandhyala, *Member, IEEE*, and Chi-Te Chen, *Student Member, IEEE*

Abstract—Numerical simulation of passive microwave remote sensing of ocean surfaces has a strict requirement of accuracy. This is because the key output of the simulations is the difference of brightness temperature between a rough surface and a flat surface. Since the difference can be as small as 0.5 K, it is important to simulate the scattering and emission accurately. In this paper, we perform accurate simulations of transverse electric (TE) and transverse magnetic (TM) waves for ocean surfaces with relative permittivity $= 28.9541 + i36.8430$ at 19 GHz. Because ocean permittivity is large, we used up to 80 points per free space wavelength. Furthermore, accurate numerical integration is also performed to obtain accurate impedance matrix elements. To ensure accuracy, a matrix equation obtained from the surface integral equation formulation is solved by matrix inversion. Conservation of energy is required to be accurate to a relative error of 0.001, which corresponds to 0.3 K in brightness temperature. Numerical results are illustrated for rough surfaces with Gaussian spectrum and bandlimited ocean spectrum and bandlimited fractal surfaces. We show convergence with respect to the density of sampling points and with respect to raising the upper limit of the bandlimited ocean spectrum. Comparisons are also made with results with an impedance boundary condition approximation. Numerical results indicate that fine discretization is required for ocean-like surfaces with fine scale roughness.

Index Terms—Method of moments (MOM), microwave emissivity, ocean rough surface.

I. INTRODUCTION

PASSIVE microwave remote sensing of ocean has important applications in retrieval of ocean parameters [1]–[6]. In the past, analytical methods such as the small perturbation method (SPM) have been applied to calculate the brightness temperature of the ocean [1], [3], [6]. Analytic theory indicates that the fine scale structures of less than a wavelength have a large influence on the ocean brightness temperature.

Recently, with the advent of modern computers, numerical simulations for rough surface scattering have been performed. Most of the ocean surface simulations are concerned with radar active remote sensing [8]–[11]. There is less work on simulations for passive remote sensing. One reason is that passive remote sensing requires much more accuracy than active remote sensing. In active remote sensing, the scattering is measured in decibel scale. For passive remote sensing, the major output is the difference of emissivity or brightness temperature between

a rough ocean surface and a flat ocean surface. The difference in emission can be as small as 0.0018 or a brightness temperature of 0.5 K using a physical temperature of 283 K. Such a strict demand of accuracy is not needed for active remote sensing. For example, numerical simulations can give good results in active remote sensing in dB scale and give poor results in passive remote sensing, because energy conservation is not obeyed well in the simulations. Thus, the numerical simulation method and approximations that are applied to active remote sensing may not be suitable for passive remote sensing because of the large difference in accuracy requirements. Another difficulty for ocean surfaces is that the relative permittivity can be as high as $28.9541 + i36.8430$ at 19 GHz [12]. For lossy dielectric rough surfaces with high permittivity, there can be rapid spatial variations of the dielectric medium Green's function and surface fields. This requires dense sampling to discretize the surface while applying the method of moments (MOM) to rough surface scattering problem. In the paper by Johnson *et al.* [4], the brightness temperatures for relatively smooth profile and incident wave at nadir were calculated. For example, the maximum value of k_U , which corresponds to the high-frequency part of the ocean spectrum, was set at 403 rads/m. As k_U becomes larger, the root mean square (rms) slope of rough surfaces will increase, because the fine scale structures have larger rms slope. More number of points per wavelength is required for some fine scale structures. Accurate near field integration to calculate impedance matrix elements is also necessary to satisfy the accuracy requirement. In the paper, We present accurate numerical results of ocean microwave emission. We give explicit equations for numerical integration to obtain impedance matrix elements for the dual integral equations and for impedance boundary conditions. We explore the accuracy for different situations. We use k_U up to 6000 rads/m at an incident angle of 50° . The energy conservation check is to within a relative error of 0.001 for both transverse electric (TE) and transverse magnetic (TM) waves, which corresponds to 0.3 K in brightness temperature. Simulations are based on a fine discretization of 40–80 points per wavelength. Near-field integrations are also performed. We also make comparisons of the results with the impedance boundary condition, which is a popular approximation method in active remote sensing [10]. Accuracy of numerical simulations is indicated by the ΔT_B , which is the difference between a rough surface and a flat surface. Many algorithms for fast solutions have been proposed (the sparse-matrix canonical grid method [SMCG] [13], [14], the physical-based two-grid method [PBTG] [15], [16], and the fast multipole method [FMM] [17]). Analytical methods can also be used

Manuscript received October 24, 2000; revised March 14, 2001. This work was supported by the Office of Naval Research under Grant N00014-99-1-0190.

The authors are with the Department of Electrical Engineering, University of Washington, Seattle, WA 98195-2500 USA (e-mail: lzhou@ee.washington.edu).

Publisher Item Identifier S 0196-2892(01)05475-4.

such as the small perturbation method [20]. These are not used in this paper, because the goal of the paper is to solve Maxwell equations exactly and calculate emissivity to within a relative error of 0.001 in energy conservation.

II. METHOD OF MOMENTS (MOM) WITH NUMERICAL INTEGRATION FOR IMPEDANCE MATRIX ELEMENTS

Consider a tapered plane wave, $\psi_{inc}(x, z)$, impinging upon a one-dimensional (1-D) rough surface with a random height profile $z = f(x)$. The incident wave is

$$\psi_{inc}(x, z) = e^{ik(x \sin \theta_i - z \cos \theta_i)(1+w(x, y))} e^{-(x+z \tan \theta_i)^2/g^2} \quad (1)$$

where

$$w = \frac{2(x+z \tan \theta_i)^2 - 1}{(kg \cos \theta_i)^2}. \quad (2)$$

θ_i is incident angle, k is the wave-number of the free space, and g is the parameter that can be changed to control the tapering of the incident wave.

For the two-media problem, we have TE or TM waves impinging upon a dielectric media (Fig. 1). Let ψ and ψ_1 denote the wave functions for the upper medium and lower medium, respectively. For the TE case, $\vec{E} = \hat{y}\psi$, and $\hat{n} \times \vec{H} = -1/(i\omega\mu)\hat{y}\hat{n} \cdot \nabla\psi$. For the TM case, $\vec{H} = \hat{y}\psi$, and $\vec{E} \times \hat{n} = -1/(i\omega\epsilon)\hat{y}\hat{n} \cdot \nabla\psi$. They satisfy the following dual surface integral equations [18]:

$$\int dS' g(\vec{r}', \vec{r}) \hat{n}' \cdot \nabla' \psi(\vec{r}') + \frac{\psi(\vec{r})}{2} - \int_P dS' \psi(\vec{r}') \hat{n}' \cdot \nabla' g(\vec{r}', \vec{r}) = \psi_{inc}(\vec{r}) \quad (3)$$

$$\int dS' g_1(\vec{r}', \vec{r}) \rho \hat{n}' \cdot \nabla' \psi(\vec{r}') - \frac{\psi(\vec{r})}{2} - \int_P dS' \psi(\vec{r}') \hat{n}' \cdot \nabla' g_1(\vec{r}', \vec{r}) = 0 \quad (4)$$

where \int_P denotes a principle value of integral and g and g_1 are the two-dimensional (2-D) Green's functions of the upper and lower medium, which are given by $g(\vec{r}, \vec{r}') = (i/4)H_0^{(1)}(k|\vec{r} - \vec{r}'|)$ and $g_1(\vec{r}, \vec{r}') = (i/4)H_0^{(1)}(k_1|\vec{r} - \vec{r}'|)$. $H_0^{(1)}$ is the zeroth order Hankel function of the first kind, and k_1 is the wave-number of the lower medium. The boundary condition on the surface S give $\psi_1(\vec{r}') = \psi(\vec{r}')$ and $\hat{n}' \cdot \nabla' \psi_1(\vec{r}') = \rho \hat{n}' \cdot \nabla' \psi(\vec{r}')$, where

$$\rho = \begin{cases} 1, & \text{for the TE case} \\ \frac{\epsilon_1}{\epsilon}, & \text{for the TM case.} \end{cases} \quad (5)$$

By using the MOM with pulse basis functions and point matching, the integral equations are discretized and given as

$$\sum_{n=1}^N A_{mn} u(x_n) + \sum_{n=1}^N B_{mn} \psi(x_n) = \psi_{inc}(x_m) \quad (6)$$

$$\sum_{n=1}^N A_{mn}^{(1)} \rho u(x_n) + \sum_{n=1}^N B_{mn}^{(1)} \psi(x_n) = 0 \quad (7)$$

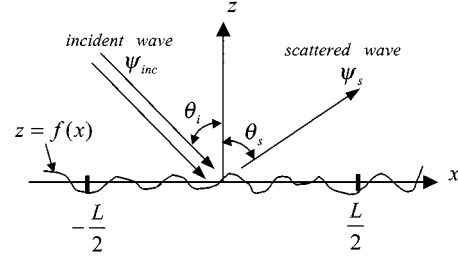


Fig. 1. Geometrical configuration for thermal emission from random rough surface.

where

$$u(x') = \sqrt{1 + \left(\frac{df(x')}{dx'}\right)^2} (\hat{n}' \cdot \nabla' \psi(\vec{r}'))_{z'=f(x')}. \quad (8)$$

For $n \neq m$

$$A_{mn} = \int_{x_n - (\Delta x/2)}^{x_n + (\Delta x/2)} dx' K(x_m, x') \quad (9)$$

$$A_{mn}^{(1)} = \int_{x_n - (\Delta x/2)}^{x_n + (\Delta x/2)} dx' K_1(x_m, x') \quad (10)$$

$$B_{mn} = - \int_{x_n - (\Delta x/2)}^{x_n + (\Delta x/2)} dx' K_N(x_m, x') \quad (11)$$

$$B_{mn}^{(1)} = - \int_{x_n - (\Delta x/2)}^{x_n + (\Delta x/2)} dx' K_{1N}(x_m, x') \quad (12)$$

where the kernels are

$$K(x, x') = \frac{i}{4} H_0^{(1)} \left(k \sqrt{(x-x')^2 + (f(x) - f(x'))^2} \right) \quad (13)$$

$$K_N(x, x') = \sqrt{1 + \left(\frac{df(x')}{dx'}\right)^2} \cdot (\hat{n}' \cdot \nabla' g(\vec{r}, \vec{r}'))_{z'=f(x'), z=f(x)} = \frac{ik}{4} \frac{H_1^{(1)} \left(k \sqrt{(x-x')^2 + (f(x) - f(x'))^2} \right)}{\sqrt{(x-x')^2 + (f(x) - f(x'))^2}} \cdot \left[\frac{df(x')}{dx'} (x' - x) - (f(x') - f(x)) \right] \quad (14)$$

$$K_1(x, x') = g_1(x, f(x); x', f(x')) = \frac{i}{4} H_0^{(1)} \left(k_1 \sqrt{(x-x')^2 + (f(x) - f(x'))^2} \right) \quad (15)$$

$$K_{1N}(x, x') = \frac{ik_1}{4} \frac{H_1^{(1)} \left(k_1 \sqrt{(x-x')^2 + (f(x) - f(x'))^2} \right)}{\sqrt{(x-x')^2 + (f(x) - f(x'))^2}} \cdot \left[\frac{df(x')}{dx'} (x' - x) - (f(x') - f(x)) \right]. \quad (16)$$

For self-patch terms, $m = n$

$$A_{mm} = \tilde{A}_{mm} + \frac{i\Delta x}{4} \left[1 + \frac{i2}{\pi} \ln \left(\frac{\gamma k}{4e} \Delta l_m \right) \right] \quad (17)$$

$$A_{mm}^{(1)} = \tilde{A}_{mm}^{(1)} + \frac{i\Delta x}{4} \left[1 + \frac{i2}{\pi} \ln \left(\frac{\gamma k_1}{4e} \Delta l_m \right) \right] \quad (18)$$

$$B_{mm} = \tilde{B}_{mm} + \frac{1}{2} \quad (19)$$

$$B_{mm}^{(1)} = \tilde{B}_{mm}^{(1)} - \frac{1}{2} \quad (20)$$

in which

$$\begin{aligned} \tilde{A}_{mm} = & \int_{x_m - (\Delta x/2)}^{x_m + (\Delta x/2)} dx' \frac{i}{4} H_0^{(1)} \\ & \cdot \left(k \sqrt{(x' - x_m)^2 + (f(x') - f(x_m))^2} \right) \\ & - \frac{i}{4} \left[1 + i \frac{2}{\pi} \ln \right. \\ & \left. \cdot \left(\frac{\gamma}{2} k \sqrt{(x' - x_m)^2 + (f(x') - f(x_m))^2} \right) \right] \end{aligned} \quad (21)$$

$$\begin{aligned} \tilde{A}_{mm}^{(1)} = & \int_{x_m - (\Delta x/2)}^{x_m + (\Delta x/2)} dx' \frac{i}{4} H_0^{(1)} \\ & \cdot \left(k_1 \sqrt{(x' - x_m)^2 + (f(x') - f(x_m))^2} \right) \\ & - \frac{i}{4} \left[1 + i \frac{2}{\pi} \ln \right. \\ & \left. \cdot \left(\frac{\gamma}{2} k_1 \sqrt{(x' - x_m)^2 + (f(x') - f(x_m))^2} \right) \right] \end{aligned} \quad (22)$$

$$\begin{aligned} \tilde{B}_{mm} = & - \int_{x_m - (\Delta x/2)}^{x_m + (\Delta x/2)} dx' \frac{ik}{4} \\ & \cdot \frac{H_1^{(1)} \left(k \sqrt{(x_m - x')^2 + (f(x_m) - f(x'))^2} \right)}{\sqrt{(x_m - x')^2 + (f(x_m) - f(x'))^2}} \\ & \cdot \left[\frac{df(x')}{dx'} (x' - x_m) - (f(x') - f(x_m)) \right] \end{aligned} \quad (23)$$

$$\begin{aligned} \tilde{B}_{mm}^{(1)} = & - \int_{x_m - (\Delta x/2)}^{x_m + (\Delta x/2)} dx' \frac{ik_1}{4} \\ & \cdot \frac{H_1^{(1)} \left(k_1 \sqrt{(x_m - x')^2 + (f(x_m) - f(x'))^2} \right)}{\sqrt{(x_m - x')^2 + (f(x_m) - f(x'))^2}} \\ & \cdot \left[\frac{df(x')}{dx'} (x' - x_m) - (f(x') - f(x_m)) \right] \end{aligned} \quad (24)$$

$$\Delta l_m = \Delta x \sqrt{1 + (f'(x_m))^2}. \quad (25)$$

III. INTEGRAL EQUATION FORMULATION USING IMPEDANCE BOUNDARY CONDITIONS

The impedance boundary condition is a common approximation to the two media problem when the lower medium is lossy. Its approximation is similar to that of the transmission line concept in which the voltage is equal to the product of the impedance and the current. In terms of wave reflection by a lossy medium, the impedance boundary condition is

$$\bar{E}_{\text{tan}} = \eta_1 \bar{J}_s = \eta_1 \hat{n} \times \bar{H} \quad (26)$$

where

\bar{E}_{tan} tangential electric field vector;
 \bar{J}_s surface electric current;
 $\eta_1 = \sqrt{\mu/\epsilon_1}$ wave impedance of the lower medium.

The surface integral equation is

$$\begin{aligned} & \int dS' g(\bar{r}', \bar{r}) \hat{n}' \cdot \nabla' \psi(\bar{r}') + \frac{\psi(\bar{r})}{2} \\ & - \int_P dS' \psi(\bar{r}') \hat{n}' \cdot \nabla' g(\bar{r}', \bar{r}) = \psi_{\text{inc}}(\bar{r}) \end{aligned} \quad (27)$$

where \int_P is the principal value integral.

For TE waves, ψ represents electric field and the surface integral equation (27) is an electric field integral equation (EFIE), while for TM waves, ψ represents magnetic field and it is a magnetic field integral equation (MFIE). We next derive a relation between ψ and $\hat{n} \cdot \nabla \psi$ using impedance boundary conditions.

For TM case, taking the cross product of both sides of (26) with the normal vector, we have

$$-\hat{n} \times \bar{E}_{\text{tan}} = \bar{M}_s = -\eta_1 \hat{n} \times \bar{J}_s \quad (28)$$

where \bar{M}_s is the surface magnetic current. Thus, the boundary condition becomes

$$\hat{n} \cdot \nabla \psi(\bar{r}) = -ik^2 \frac{\psi(\bar{r})}{k_1} \quad (29)$$

and the surface integral equation becomes

$$\begin{aligned} & -i \frac{k^2}{k_1} \int dS' g(\bar{r}', \bar{r}) \psi(\bar{r}') + \frac{\psi(\bar{r})}{2} \\ & - \int_P dS' \psi(\bar{r}') \hat{n}' \cdot \nabla' g(\bar{r}', \bar{r}) = \psi_{\text{inc}}(\bar{r}). \end{aligned} \quad (30)$$

The surface unknown is $\psi(\bar{r})$.

For TE case, the impedance boundary condition in terms of the wave function becomes

$$\frac{1}{ik_1} \hat{n} \cdot \nabla \psi(\bar{r}) = -\psi(\bar{r}). \quad (31)$$

Thus, the surface integral equation becomes

$$\begin{aligned} & \int dS' g(\bar{r}', \bar{r}) \hat{n}' \cdot \nabla' \psi(\bar{r}') - \frac{\hat{n} \cdot \nabla \psi(\bar{r})}{2ik_1} + \frac{1}{ik_1} \\ & \cdot \int_P dS' (\hat{n}' \cdot \nabla' g(\bar{r}', \bar{r})) (\hat{n}' \cdot \nabla' \psi(\bar{r}')) = \psi_{\text{inc}}(\bar{r}) \end{aligned} \quad (32)$$

and the surface unknown is $u(\bar{r}) = \sqrt{1 + (f'(x))^2} \hat{n} \cdot \bar{\nabla} \psi(\bar{r})$.

When applying MOM to solve these integral equations, matrix equations can be given as

$$\sum_{n=1}^N Q_{mn}^{\text{TM}} \psi(x_n) = \psi_{\text{inc}}(x_m), \quad \text{for TM case} \quad (33)$$

and

$$\sum_{n=1}^N Q_{mn}^{\text{TE}} u(x_n) = \psi_{\text{inc}}(x_m), \quad \text{for TE case} \quad (34)$$

in which

$$Q_{mn}^{\text{TM}} = -i \frac{k^2}{k_1} \sqrt{1 + (f'(x_n))^2} A_{mn} + B_{mn} \quad (35)$$

$$Q_{mn}^{\text{TE}} = A_{mn} + \frac{1}{ik_1 \sqrt{1 + (f'(x_n))^2}} B_{mn}. \quad (36)$$

A_{mn} , B_{mn} , and $u(x)$ are defined in Section II, and matrix elements are computed accurately by using numerical integration.

Using the impedance boundary condition, the emissions of flat dielectric surfaces for TE and TM incident waves are given as

$$e_{\text{TE}} = 1 - |R_{\text{TE}}|^2, \quad \text{for TE waves} \quad (37)$$

$$e_{\text{TM}} = 1 - |R_{\text{TM}}|^2, \quad \text{for TM waves} \quad (38)$$

where

$$R_{\text{TE}} = \frac{k_{iz} - k_1}{k_{iz} + k_1} \quad (39)$$

$$R_{\text{TM}} = \frac{k_{iz} - k^2/k_1}{k_{iz} + k^2/k_1}. \quad (40)$$

IV. EMISSIVITY AND BRIGHTNESS TEMPERATURE

For a penetrable medium, absorptivity $a(\theta_i)$ and reflectivity $r(\theta_i)$ can be calculated in term of the surface fields

$$a(\theta_i) = \frac{P_a}{P_{inc}} = \frac{\text{Im} \int dx \psi(x) u^*(x)}{k \cos \theta_i g \sqrt{\frac{\pi}{2}} \left\{ 1 - \frac{1 + 2 \tan^2 \theta_i}{2k^2 g^2 \cos^2 \theta_i} \right\}} \quad (41)$$

$$r(\theta_i) = \frac{P_s}{P_{inc}} = \frac{\text{Im} \int dx \psi_s(x) u_s^*(x)}{k \cos \theta_i g \sqrt{\frac{\pi}{2}} \left\{ 1 - \frac{1 + 2 \tan^2 \theta_i}{2k^2 g^2 \cos^2 \theta_i} \right\}} \quad (42)$$

where the surface scattered fields are

$$\psi_s(x) = \psi(x) - \psi_{inc}(x) \quad (43)$$

$$u_s(x) = u(x) - u_{inc}(x). \quad (44)$$

In passive remote sensing, the brightness temperature T_B of the medium is measured at incident angle θ_i . The brightness temperature is equal to

$$T_B(\theta_i) = e(\theta_i)T \quad (45)$$

where emissivity $e(\theta_i)$ is equal to $a(\theta_i)$, and T is the physical temperature of the medium in K.

V. ROUGH SURFACE PROFILES AND GENERATION

In the simulation, we use three models of random rough surfaces to demonstrate the accuracy problem in passive remote sensing. The models are the following.

- 1) It is assumed that the ocean surface is a Gaussian process with spectrum given below. The small-scale wind-induced surfaces are described by an empirical sea surface spectrum proposed by Durden and Vesecky [7]. We used a 1-D analog of a 2-D spectrum. In the 1-D spectrum

$$W(|k_x|) = \frac{S(|k_\rho|)}{2} \quad (46)$$

$$S(k_\rho) = \begin{cases} \frac{a_0}{k_\rho^3} \left(\frac{bk_\rho u_*^2}{g_*} \right)^{a \log_{10}(k_\rho/K_j)} & k_\rho > k_j \\ \frac{b_0}{k_\rho^3} e^{(-0.74(k_c/k_\rho)^2)} & k_\rho \leq k_j. \end{cases} \quad (47)$$

Parameters used are the same as referred in [1], [3], and [7]. We use the magnitude parameter $a_0 = 0.008$ and wind speed $U_{5,0} = 10$ m/s. The spectrum is further band-limited between k_L and k_U , which control ocean surface rms height and variance of slope that are appropriate in microwave emission problems.

- 2) The random rough surface is generated by using Gaussian process with a Gaussian spectrum, which is given as

$$W(k_x) = \frac{1}{2\pi} \int_{-\infty}^{\infty} d\tau e^{-ik_x \tau} h^2 C(\tau) = \frac{h^2 l e^{-(k_x^2 l^2)/4}}{2\sqrt{\pi}} \quad (48)$$

where h is the rms height, and l is correlation length.

TABLE I

COMPARISON OF EMISSIVITIES WITH VARIOUS SURFACE LENGTHS FOR TE AND TM POLARIZATIONS USING OCEAN SPECTRUM WITH $k_L = 100$ rads/m, $k_U = 4000$ rads/m, AND 60 TO 80 points/ λ DISCRETIZATION. * REPRESENTS THE CORRECT RESULT

Polar.	Surface length(λ)	Emission	Energy cons. $a(\theta_i) + r(\theta_i)$	Emissivity of flat surface	$T_B(K)$	$\Delta T_B(\text{rough} - \text{flat surface})$
TE	8	0.28914	0.99384	0.28728	81.83	0.53
TE	16	0.29738	0.99974	0.28728	84.16	2.86
TE	20	0.29695*	1.00016	0.28728	84.04	2.74*
TM	8	0.57340	1.0006	0.55927	162.27	4.00
TM	16	0.56778	1.00084	0.55927	160.68	2.41
TM	20	0.56823*	1.00096	0.55927	160.81	2.53*

- 3) For fractal surface, we can use the Weierstrass-Mandelbrot function [19]

$$f(x) = hC_N \sum_{n=0}^{N_f-1} b^{(S-2)n} \sin(K_0 b^n x + \Phi_n) \quad (49)$$

where

N_f number of tones;

S fractal dimension ($1 \leq S < 2$);

h equivalent rms height.

Φ_n is a Gaussian random variable uniformly distributed between 0 and $2\pi \cdot 2\pi \cdot \text{rand}(N_f, 1)$. The bandlimit can be controlled by $K_0 = k_L$ and $K_0 b^{N_f-1} = k_U$. $k_L = 100$ and $k_U = 4000$ are used in the simulation. Note that a fractal surface as given by (49) is not a Gaussian process.

Ocean surface is usually assumed to be a Gaussian process with power law spectrum. It has not been rigorously verified that the ocean surface is a Gaussian process. The fractal model is a non-Gaussian process. Comparing profiles generated by three models, it can be found that the fractal surface is spikier. It has more fine scale structures [20], [21].

VI. NUMERICAL RESULTS AND DISCUSSION

The important result to compare is

$$\Delta T_B = T_B(\text{rough surface}) - T_B(\text{flat surface}). \quad (50)$$

We also carry out numerical energy conservation by calculating $a(\theta_i)$ and $r(\theta_i)$ using (41) and (42) and see whether $a(\theta_i) + r(\theta_i)$ is equal to unity. The dielectric constant of $28.9541 + i36.8430$ is assumed in this work. Frequency 19 GHz and viewing angle 50° are used, and physical temperature T is 283 K. Table I presents the emissivity for both TE and TM waves with various surface lengths. Based on the energy conservation check, a surface length of 8 wavelengths is not large enough to give correct results. A surface length of 20 wavelengths is used in all subsequent simulations. The tapering parameter of the incident wave is chosen as $g = L/4$.

To demonstrate the significance of performing a rigorous near-field integration, sample results are presented in Table II that illustrate a large improvement in the TM case when integration is considered. For Dirichlet problem, the kernel is $H_0^{(1)}$,

TABLE II

COMPARISON OF EMISSIVITIES WITH AND WITHOUT NEAR-FIELD INTEGRATION FOR TE AND TM WAVES USING OCEAN SPECTRUM WITH $k_L = 100$ rads/m, $k_U = 4000$ rads/m, AND 60 TO 80 points/ λ DISCRETIZATION. * REPRESENTS THE CORRECT RESULT

Near field int. performed	Polar.	Emissivity	Energy cons. $a(\theta_i) + r(\theta_i)$	Emissivity of flat surface	$T_B(K)$	$\Delta T_B(\text{rough} - \text{flat surface})$
YES	TE	0.29695*	1.00016	0.28728	84.04	2.74*
NO	TE	0.29696	0.9997	0.28728	84.04	2.74
YES	TM	0.56823*	1.00096	0.55927	160.81	2.54*
NO	TM	0.56124	0.9968	0.55927	158.83	0.56

TABLE III

EMISSIVITY WITH VARIOUS SAMPLING DENSITY (NUMBER OF points/ λ). $k_L = 100$ rads/m, AND $k_U = 4000$ rads/m

No. of points/ λ	Polar.	Emissivity	Energy cons. $a(\theta_i) + r(\theta_i)$	Emissivity of flat surface	$T_B(K)$	$\Delta T_B(\text{rough} - \text{flat surface})$
10	TE	0.30400	1.0189	0.28728	86.03	4.73
40	TE	0.29710	1.00050	0.28728	84.08	2.78
60	TE	0.29695	1.00016	0.28728	84.04	2.74
80	TE	0.29686	0.999968	0.28728	84.01	2.71
10	TM	0.56097	0.99511	0.55927	158.75	0.48
40	TM	0.56894	1.00155	0.55927	161.01	2.74
60	TM	0.56849	1.00121	0.55927	160.88	2.61
80	TM	0.56823	1.00096	0.55927	160.81	2.54

while for the Neumann problem, the kernel is $H_1^{(1)}$, which is more singular. The TM case is dominated by the Neumann kernel, so that numerical integration is more important. During calculating the matrix elements, numerical integration is performed over the upper and lower medium Green's functions for the points within a radius of 2.0 free space wavelengths around the testing points. Within the domain of each pulse basis function, we use 25 points to perform numerical integration.

In Table III, the ocean rough surface is generated using 240 points/wavelength. Numerical simulations of scattering and emission are performed for one realization on the same profile from ten to 80 points per wavelength in the sparse grid. $k_L = 100$ rads/m, and $k_U = 4000$ rads/m. It is shown that results converge and accuracy requirement is satisfied with 40 points per wavelength discretization for TE polarization, while 80 points per wavelength are required for TM polarization.

In Table IV, k_U is chosen to be 400 rads/m, 1000 rads/m, 4000 rads/m and 6000 rads/m with fixed $k_L = 100$ rads/m. The electromagnetic wave-number-surface rms height products ($k\sigma$) for these three cases were 0.311 30, 0.322 57, 0.324 04, and 0.324 06, respectively. Results show the importance of the Bragg scattering contribution to observed brightness temperatures and emissivities. We also list some results calculated by using the impedance boundary condition. Comparing the results in Tables V and IV, we find that good agreement is achieved between the results using the impedance boundary condition and the dual integral equation when k_U is small. However, as k_U

TABLE IV

EMISSIVITY AND BRIGHTNESS TEMPERATURE WITH VARIOUS VALUES OF k_U . $k_L = 100$ rads/m

Polar.	k_U (rads/m)	Emission	Energy cons. $a(\theta_i) + r(\theta_i)$	Emissivity of flat surface	$T_B(K)$	$\Delta T_B(\text{rough} - \text{flat surface})$
TE	400	0.29358	1.00010	0.28728	83.08	1.78
TE	1000	0.29507	1.00006	0.28728	83.50	2.20
TE	4000	0.29695	1.00016	0.28728	84.04	2.74
TE	6000	0.29709	1.00011	0.28728	84.08	2.78
TM	400	0.56250	1.00010	0.55927	159.19	0.91
TM	1000	0.56513	1.00024	0.55927	159.93	1.66
TM	4000	0.56823	1.00096	0.55927	160.81	2.54
TM	6000	0.56862	1.00110	0.55927	160.92	2.65

TABLE V

EMISSIVITY AND BRIGHTNESS TEMPERATURE WITH VARIOUS VALUES OF k_U USING IMPEDANCE BOUNDARY CONDITIONS. THE PARAMETERS USED ARE THE SAME AS IN TABLE IV

Polar.	k_U (rads/m)	Emission	Energy cons. $a(\theta_i) + r(\theta_i)$	Emissivity of flat surface	$T_B(K)$	$\Delta T_B(\text{rough} - \text{flat surface})$
TE	400	0.29299	1.0001	0.28684	82.92	1.74
TE	1000	0.29403	1.0001	0.28684	83.21	2.03
TE	4000	0.29403	1.0001	0.28684	83.21	2.03
TE	6000	0.29386	1.0002	0.28684	83.16	1.99
TM	400	0.56286	1.0001	0.55984	159.29	0.85
TM	1000	0.56557	1.0004	0.55984	160.06	1.62
TM	4000	0.56879	1.0016	0.55984	160.97	2.53
TM	6000	0.56935	1.0018	0.55984	161.13	2.69

TABLE VI

EMISSIVITY AND BRIGHTNESS TEMPERATURE FOR GAUSSIAN ROUGH SURFACE WITH rms HEIGHT $h = 0.2\lambda$ AND CORRELATION LENGTH $l = 0.2\lambda$

Method	Polar.	Emission	Energy cons. $a(\theta_i) + r(\theta_i)$	Emissivity of flat surface	$T_B(K)$	$\Delta T_B(\text{rough} - \text{flat surface})$
Dual	TE	0.42639	1.00067	0.28728	120.67	39.37
Dual	TM	0.63463	1.0084	0.55927	179.60	21.33
Impedance	TE	0.40160	1.0007	0.28684	113.65	32.48
Impedance	TM	0.63428	1.011	0.55984	179.50	21.07

TABLE VII

EMISSIVITY AND BRIGHTNESS TEMPERATURE FOR FRACTAL SURFACE. $K_0 = k_L = 100$ rads/m, AND $K_0 b^{Nf-1} = k_U = 4000$ rads/m

Method	Polar.	Emission	Energy cons. $a(\theta_i) + r(\theta_i)$	Emissivity of flat surface	$T_B(K)$	$\Delta T_B(\text{rough} - \text{flat surface})$
Dual	TE	0.32536	0.99974	0.28728	92.08	10.78
Dual	TM	0.60870	1.0147	0.55927	172.26	13.99
Impedance	TE	0.29923	1.0010	0.28684	84.68	3.51
Impedance	TM	0.60536	1.0149	0.55984	171.32	12.88

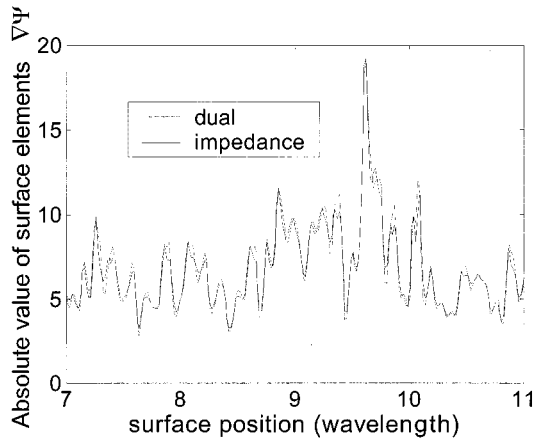


Fig. 2. Values of matrix elements in term of $|\nabla\psi(\vec{r})|$ on the fractal rough surface with $k_L = 100$ rads/m and $k_U = 4000$ rads/m for TE waves, using the dual integral equation and the impedance boundary approximation.

and roughness of surfaces increase, the differences of the results between two methods become larger, especially for TE case, which can be found in Tables VI and VII. In Table VI, rms height $h = 0.2\lambda$ and correlation length $l = 0.2\lambda$ are used in the simulation with Gaussian spectrum. Table VII gives emissivities and brightness temperatures for fractal surfaces using the dual integral equation and the impedance boundary condition. For fractal surfaces, the number of tones (N_f) is 100, and the fractal dimension s is 1.5. The equivalent rms height $h = 0.051572\lambda$ is the same as that chosen in the ocean spectrum $k_L = 100$ rads/m, and $k_U = 4000$ rads/m. Using the fractal surface, the surface currents in term of $|\nabla\psi(\vec{r})|$ are plotted in Fig. 2. It is found that there are some differences in the surface currents. As indicated in Table VII, the difference in emissivity between the dual integral equation and the impedance boundary condition is large for fractal surfaces.

VII. CONCLUSION

Accurate simulations for 2-D scattering problem are presented. To satisfy stringent accuracy requirements, near-field integration and fine discretization of surfaces are necessary for fine scale roughness. All numerical results are validated with an energy conservation check. Numerical results show the importance of the Bragg scattering contribution to brightness temperatures and emissivities for fine scale structures. It is also shown that the impedance boundary condition could give correct results for smooth rough surfaces. However, with the presence of fine scale structures with small radii of curvatures, impedance boundary conditions give errors in the emissivity for TE case.

REFERENCES

- [1] S. H. Yueh, R. Kwok, F. K. Li, S. V. Nghiem, W. J. Wilson, and J. A. Kong, "Polarimetric passive remote sensing of ocean wind vector," *Radio Sci.*, pp. 799–814, 1994.
- [2] S. H. Yueh, W. J. Wilson, F. K. Li, S. V. Nghiem, and W. B. Ricketts, "Polarimetric measurements of sea surface brightness temperatures using an aircraft K-band radiometer," *IEEE Trans. Geosci. Remote Sensing*, vol. 33, pp. 85–92, Jan. 1995.
- [3] S. H. Yueh, "Modeling of wind direction signals in polarimetric sea surface brightness temperatures," *IEEE Trans. Geosci. Remote Sensing*, vol. 35, pp. 1400–1418, 1997.

- [4] J. T. Johnson, R. T. Shin, J. A. Kong, L. Tsang, and K. Pak, "A numerical study of ocean polarimetric thermal emission," *IEEE Trans. Geosci. Remote Sensing*, vol. 37, pp. 8–20, Jan. 1999.
- [5] S. Q. Li, C. H. Chan, L. Tsang, Q. Li, and L. Zhou, "Parallel implementation of the sparse matrix/canonical grid method for the analysis of two-dimensional random rough surfaces (three-dimensional scattering problem) on a Beowulf system," *IEEE Trans. Geosci. Remote Sensing*, vol. 38, pp. 1600–1608, July 2000.
- [6] V. G. Irisov, "Azimuthal variations of the microwave radiation from a slightly non-Gaussian sea surface," *Radio Science*, vol. 35, no. 1, pp. 65–82, Jan.–Feb. 2000.
- [7] S. P. Durden and J. F. Vesecky, "A physical radar cross section model for a wind driven sea with swell," *IEEE J. Oceanic Eng.*, vol. OE-10, pp. 445–451, 1985.
- [8] J. C. West, "Integral equation formulation for iterative calculation of scattering from lossy rough surfaces," *IEEE Trans. Geosci. Remote Sensing*, vol. 38, pp. 1609–1615, July 2000.
- [9] J. V. Toporkov and G. S. Brown, "Numerical simulations of scattering from time-varying, randomly rough surfaces," *IEEE Trans. Geosci. Remote Sensing*, vol. 38, pp. 1616–1625, July 2000.
- [10] H. T. Chou and J. T. Johnson, "Formulation of forward-backward method using novel spectral acceleration for the modeling of scattering from impedance rough surfaces," *IEEE Trans. Geosci. Remote Sensing*, vol. 38, pp. 605–607, Jan. 2000.
- [11] J. T. Johnson, J. A. Kong, R. T. Shin, S. H. Yueh, S. V. Nghiem, and R. Kwok, "Polarimetric thermal emission from rough ocean surfaces," *J. Electromagn. Waves Applicat.*, vol. 8, no. 1, pp. 43–59, 1994.
- [12] J. P. Hollinger, "DMSP special sensor microwave/imager calibration validation," Final Rep., Naval Res. Lab., Washington, DC, 1989.
- [13] K. Pak, L. Tsang, C. H. Chan, and J. Johnson, "Backscattering enhancement of vector electromagnetic waves from two-dimensional perfectly conducting random rough surfaces with the sparse-matrix canonical grid method," *J. Opt. Soc. Amer. A*, vol. 12, pp. 2491–2499, Nov. 1995.
- [14] K. Pak, L. Tsang, and J. Johnson, "Numerical simulations and backscattering enhancement of electromagnetic waves from two-dimensional dielectric random rough surfaces with the sparse-matrix canonical grid method," *J. Opt. Soc. Amer. A*, vol. 14, pp. 1515–1529, July 1997.
- [15] L. Tsang and Q. Li, "Numerical solution of scattering of waves by lossy dielectric surfaces using a physics-based two-grid method," *Microwave Opt. Technol. Lett.*, vol. 16, pp. 356–364, Dec. 20, 1997.
- [16] Q. Li, C. H. Chan, and L. Tsang, "Monte-Carlo simulations of wave scattering from lossy dielectric random rough surfaces using the physics-based two-grid method and canonical grid method," *IEEE Trans. Antennas Propagat.*, vol. 47, pp. 752–763, Apr. 1999.
- [17] E. Michielsen and W. C. Chew, "Fast steepest descent path algorithm for analyzing scattering from two-dimensional objects," *Radio Sci.*, vol. 31, pp. 1215–1224, Sept.–Oct. 1996.
- [18] L. Tsang, J. A. Kong, and R. Shin, *Theory of Microwave Remote Sensing*. New York: Wiley, 1985.
- [19] F. Berizzi, E. D. Dalle Mese, and G. Pinelli, "One dimensional fractal model of the sea surface," *Proc. Inst. Elect. Eng.*, vol. 146, pp. 55–64, 1999.
- [20] L. Tsang, J. A. Kong, and K.H. Ding, *Scattering of Electromagnetic Waves: Theories and Applications*. New York: Wiley, 2000.
- [21] L. Tsang, J. A. Kong, K. H. Ding, and C. Ao, *Scattering of Electromagnetic Waves: Numerical Simulations*. New York: Wiley, 2001, to be published.



Lin Zhou (S'00) received the B.Eng. degree in electrical engineering from the University of Electronic Science and Technology of China, Chengdu, in 1989, and the M.Eng. degree from the National University of Singapore, Singapore, in 1999. He is currently pursuing the Ph.D. degree at the University of Washington, Seattle.

Since 1999, he has been with the Department of Electrical Engineering, University of Washington, as a Research Assistant. From 1989 to 1996, he was with the Communication Division, the Civil Aviation Administration of China, Henan, China, as an Engineer. His current interests include theoretical and numerical studies of electromagnetic wave scattering and propagation in random media and remote sensing.



Leung Tsang (S'73–M'75–SM'85–F'90) was born in Hong Kong. He received the S.B., S.M., E.E., and Ph.D. degrees from the Massachusetts Institute of Technology, Cambridge.

He is currently a Professor of electrical engineering with the University of Washington, Seattle. He is co-author of the book *Theory of Microwave Remote Sensing* (New York: Wiley, 1985). His current research interests include wave propagation in random media and rough surfaces, remote sensing, optoelectronics, and computational

electromagnetics.

Dr. Tsang was Editor-in-Chief of IEEE TRANSACTIONS ON GEOSCIENCE AND REMOTE SENSING from 1996 to 2001. He was the Technical Program Chairman of the 1994 IEEE Antennas and Propagation International Symposium and URSI Radio Science Meeting, the Technical Program Chairman of the 1995 Progress in Electromagnetics Research Symposium, and the General Chairman of the 1998 IEEE International Geoscience and Remote Sensing Symposium. He is a Fellow of the Optical Society of America and the recipient of the Outstanding Service Award of the IEEE Geoscience and Remote Sensing Society for 2000. He is also the Recipient of the IEEE Third Millennium Medal.



Vikram Jandhyala (M'00) received the B.Tech. degree in electrical engineering from the Indian Institute of Technology, Delhi, India, in 1993, and the M.S. and Ph.D. degrees in electrical engineering from the University of Illinois, Urbana, in 1995 and 1998, respectively.

He is currently an Assistant Professor with the Department of Electrical Engineering, University of Washington, Seattle. From 1998 to 2000, he was a Research and Development Engineer with Ansoft Corporation, Pittsburgh, PA, where he worked on

developing fast integral equation solvers for signal integrity applications. His areas of interest include computational electromagnetics and applications in scattering, high-speed circuits, remote sensing, integral equations, and fast algorithms. He is the co-developer of the steepest descent fast multipole method and of the fast multipole integral equation implementation in Ansoft's signal integrity software. He has published approximately 50 papers in refereed journals and conference proceedings. He serves as a reviewer for several IEEE journals.

Dr. Jandhyala is a recipient of a 2001 NSF CAREER Award, a 1998 Outstanding Graduate Research Award at the University of Illinois, and a 1997 IEEE Microwave Graduate Fellowship.

Chi-Te Chen (S'98) received the B.S. degree in electrical engineering from the National Taiwan University, Taipei, Taiwan, R.O.C., in 1994, and the M.S. degree from the University of Washington, Seattle, in 1996, where she is currently pursuing the Ph.D. degree.

Her research interests include theoretical and numerical studies of electromagnetic wave scattering and propagation in random media and remote sensing.